

Soft Matter

Accepted Manuscript



This is an *Accepted Manuscript*, which has been through the Royal Society of Chemistry peer review process and has been accepted for publication.

Accepted Manuscripts are published online shortly after acceptance, before technical editing, formatting and proof reading. Using this free service, authors can make their results available to the community, in citable form, before we publish the edited article. We will replace this *Accepted Manuscript* with the edited and formatted *Advance Article* as soon as it is available.

You can find more information about *Accepted Manuscripts* in the [Information for Authors](#).

Please note that technical editing may introduce minor changes to the text and/or graphics, which may alter content. The journal's standard [Terms & Conditions](#) and the [Ethical guidelines](#) still apply. In no event shall the Royal Society of Chemistry be held responsible for any errors or omissions in this *Accepted Manuscript* or any consequences arising from the use of any information it contains.

A terminally protected dipeptide: from crystal structure and self-assembly, through co-assembly with carbon-based materials, to a ternary catalyst for reduction chemistry in water

Daniela Mazzier,^a Francesco Carraro,^a Marco Crisma,^b Marzio Rancan,^c Claudio Toniolo,^{a,b} and Alessandro Moretto^{a,b}*

^aDepartment of Chemical Sciences, University of Padova, 35131 Padova, Italy

^bInstitute of Biomolecular Chemistry, Padova Unit, CNR, 35131 Padova, Italy

^cInstitute for Energetics and Interphases, CNR, 35131 Padova, Italy

e-mail: alessandro.moretto.1@unipd.it

Abstract: The terminally protected, hydrophobic dipeptide Boc-L-Cys(Me)-L-Leu-OMe (**1**) was synthesized and its 3D-structure determined by single crystal X-ray diffraction analysis. This peptide is able to hierarchically self-assemble in a variety of superstructures, including hollow rods, ranging from the nano- to the macroscale, and organogels. In addition, **1** is able to drive fullerene (C₆₀) or multiwall carbon nanotubes (MWCNTs) in an organogel by co-assembling with them. A hybrid **1**-C₆₀-MWCNTs organogel was prepared and converted (through a high vacuum-drying process) into a robust, high-volume, water insoluble, solid material where C₆₀ is well dispersed over the entire superstructure. This ternary material was successfully tested as a catalyst for: (i) the reduction reaction of water-soluble azo compounds mediated by NaBH₄ and UV-light with an overall performance remarkably better than that provided by C₆₀ alone, and (ii) the NaBH₄-mediated reduction of benzoic acid to benzyl alcohol. Our results suggest that the self-assembly properties of **1** might be related to the occurrence in its single crystal structure of a sixfold screw axis, a feature shared by most of the linear peptides known so far to give rise to nanotubes.

1. Introduction

Since J.M. Lehn's pioneering contributions, the bottom-up self-assembly strategy has emerged as one of the most applicable approaches to drive small molecule arrangements.¹⁻⁴ Following a hierarchical process, under appropriate conditions the combination of a variety of non-covalent interactions may allow properly designed molecules to form stable, ordered aggregates that can evolve into nano-, micro- and macroscale materials characterized by discrete 3D-architectures with specific shapes, dimensions and functions, exploitable in areas ranging from chemistry to materials science and medicine.^{5,6} In this connection, peptides represent powerful building blocks on the nanoscale because of their modularity, molecular diversity, which can be expanded beyond the repertoire of genetically coded amino acids, and secondary structure variety.⁷⁻¹⁷ More specifically, nanotubes and nanofibers predominate as molecular architectures among the self-assemblies formed by short, unprotected peptides¹⁸⁻²¹ of which the phenylalanine homo-dipeptide H-Phe-Phe-OH is the most extensively investigated example (for review, see ref. 7). Notably, such architectures may adsorb or entrap other molecules, thus generating ordered hybrid materials.²² Conversely, only a few examples of terminally-protected peptides, the crystal structures of which are characterized by a nanotube architecture, were reported, but their self-assembly properties have not been further explored.²³⁻²⁶

Here, we present our data on the hydrophobic, terminally protected dipeptide Boc-L-Cys(Me)-L-Leu-OMe (1) [where Boc is tert-butoxycarbonyl, Cys(Me) is S-methyl cysteine, and OMe is methoxy] (Figure 1A) that was crystallographically characterized and subsequently was found to be able to hierarchically self-assemble producing nano-, micro- and macroscale tubes and organogels that we eventually exploited to incorporate guest molecules such as gold nanoparticles, C₆₀ fullerene and multiwall carbon nanotubes (MWCNTs). Moreover, from an organogel composed of 1, C₆₀ and MWCNTs, by a simple vacuum-drying process we generated an ordered, robust, carbon-based non-covalently

assembled material, which displayed high performances when used as catalyst in reduction chemistry.

2. Materials and methods

2.1 X-Ray diffraction

(i) Single crystal X-ray diffraction data were collected with an Agilent Technologies Gemini E four-circle kappa diffractometer equipped with a 92 mm EOS CCD detector, using graphite monochromated Cu K α radiation ($\lambda = 1.54178 \text{ \AA}$). Data collection and reduction were performed with the CrysAlisPro software (Agilent Technologies). The structures were solved by *ab initio* procedures of the SIR 2002 program,²⁷ and refined by full-matrix least-squares on F^2 , using all data, by application of the SHELXL-97 program.²⁸ Additional details may be found in the *Supporting Information*. (ii) Powder X-ray diffraction measurements were carried out by means of a Bruker D8 Advance diffractometer equipped with a Göbel mirror and a Cu K α source (40 kV, 40 mA). Powder pattern indexing was performed by use of the N-TREOR²⁹ software in the framework of the EXPO2013³⁰ package.

2.2 Self-assembly investigations

(i) Self-assembly from solvent evaporation. Typically, from 500 mg to 1 g of **1** were dissolved in 10 to 20 ml of the appropriate solvent (MeOH, CH₃CN or EtOAc). The resulting clear solution was allowed to stand in a large crystallization vessels at controlled temperature (25 °C). After evaporation of the solvent macroscopic rods were obtained. (ii) Self-assembly from water/EtOAc interfacial crystallization. Typically, from 100 to 200 mg of **1** were dissolved in 10 to 20 ml of EtOAc. The resulting clear solution was gently layered over mQ water in a crystallization vessels at controlled temperature (25 °C). After evaporation of EtOAc, micrometric rods were collected from the water solution. (iii) Self-assembly from MeOH/water. Typically from 0.1 to 1 mL of a MeOH solution of **1** (2 mg/mL) were added to 1 mL of H₂O and allowed to stand in a sealed vessel for 1 to 3 days.

2.3 Organogel preparations

(i) Pristine **1**-organogel was prepared as follows. Dipeptide **1** was added in small amounts to toluene to the concentration of 85 mg/mL. Then, the resulting suspension was heated at 60 °C under sonication, for 5 min. After standing at rt, the clear solution turned into an organogel.

(ii) The **1**-C₆₀ organogel was prepared as follows. Typically, from 5 to 8 mg of C₆₀ were added to 1 mL of toluene and the suspension was heated at 70 °C up to complete solubilization. Then, 85 mg of **1** were added to the C₆₀ solution in small amounts to the concentration of 85 mg/mL. The resulting suspension was heated at 60 °C under sonication for 10 min. After standing at rt, the clear, dark-red solution turned into an organogel. (iii) The **1**-MWCNTs organogel was prepared as follows. MWCNTs, 20 mg, were suspended in 1 mL of toluene and sonicated for 5 min. Then, **1** was added to the suspension in small amounts to the concentration of 85 mg/mL. The resulting suspension was heated at 65 °C under sonication for 20 min. The black mixture gradually turned into an organogel.

2.4 **1**-C₆₀-MWCNTs composite/catalyst preparation

Typically, 5 mL of the **1**-C₆₀ organogel and 5 ml of the **1**-MWCNTs organogel (prepared as described above) were separately melted in their sol state. The two solutions were combined and heated at 75 °C under sonication for 5 min. The dark mixture gradually turned into a stable organogel. The organogel was directly dried *in vacuo*. The nanocomposite contains from 2.5 to 5 % w/w of fullerene.

2.5 Reduction of azo compounds under UV irradiation

Reduction of methyl orange (MO) was carried out in a 50 mL beaker. NaOH solution (1M, 0.5 mL), distilled water (40 mL), NaBH₄ (100 mg), and MO (200 mg) were added. Then, the **1**-C₆₀-MWCNTs catalyst (100 mg, C₆₀ as 2.5% w/w) was added to form a suspension. The reaction proceeded by stirring under UV irradiation (UV lamp, 365 nm, 50 Hz) at rt for 45 min. After the catalyst was removed by filtration, the reaction mixture was characterized

using HPLC-MS analysis. The experiment was repeated 3 times. The reduction procedure of methyl red (MR) and 4-aminoazobenzene (AZ) in water was similar to that described above.

2.6 Reduction of benzoic acid under UV irradiation

Reduction of Benzoic Acid was carried in similar condition as described for Azo compounds. The reaction proceeded by stirring under UV irradiation (UV lamp, 365 nm, 50 Hz) at rt for 3 hours. After the catalyst was removed by filtration, the reaction mixture was characterized using HPLC-MS analysis.

3. Result and discussion

3.1 X-Ray diffraction

The X-ray diffraction structure of **1** [determined on a single crystal grown from MeOH (methanol)] is illustrated in Figure 1B.³¹ The conformation adopted by both α -amino acid residues is *semi*-extended, and the N-H groups of Cys and Leu point to opposite directions. In the packing mode (Figure 1C), the (urethane) N1-H group is intermolecularly H-bonded to the $(y, -x+y, z+1/6)$ symmetry equivalent of the (urethane) O0 atom, and the (amide) N2-H group is H-bonded to the $(x-y, x, z-1/6)$ symmetry equivalent of the (amide) O1 atom (*Supporting Information*, Table S3). As a result, H-bonded molecules wrap around the sixfold screw axis along the *c* direction, each molecule being connected to the next by two H-bonds. The left-handed, supramolecular sixfold helix thus generated is characterized by a very narrow lumen, about 2.5 Å in diameter (Figure 1C, bottom). The Cys(Me) and Leu side chains, as well as the N- and C-terminal Boc and OMe groups of each molecule, are located on the external surface. Each helical row of molecules is surrounded by six counterparts (Figure 1D). Lateral stabilization between rows is provided, in addition to van der Waals interactions, by C-H \cdots O interactions taking place between the (Boc) C02-H02B group and the $(x-1, y-1, z)$ symmetry equivalent of the (methyl ester) OT atom (*Supporting Information*, Table S3).

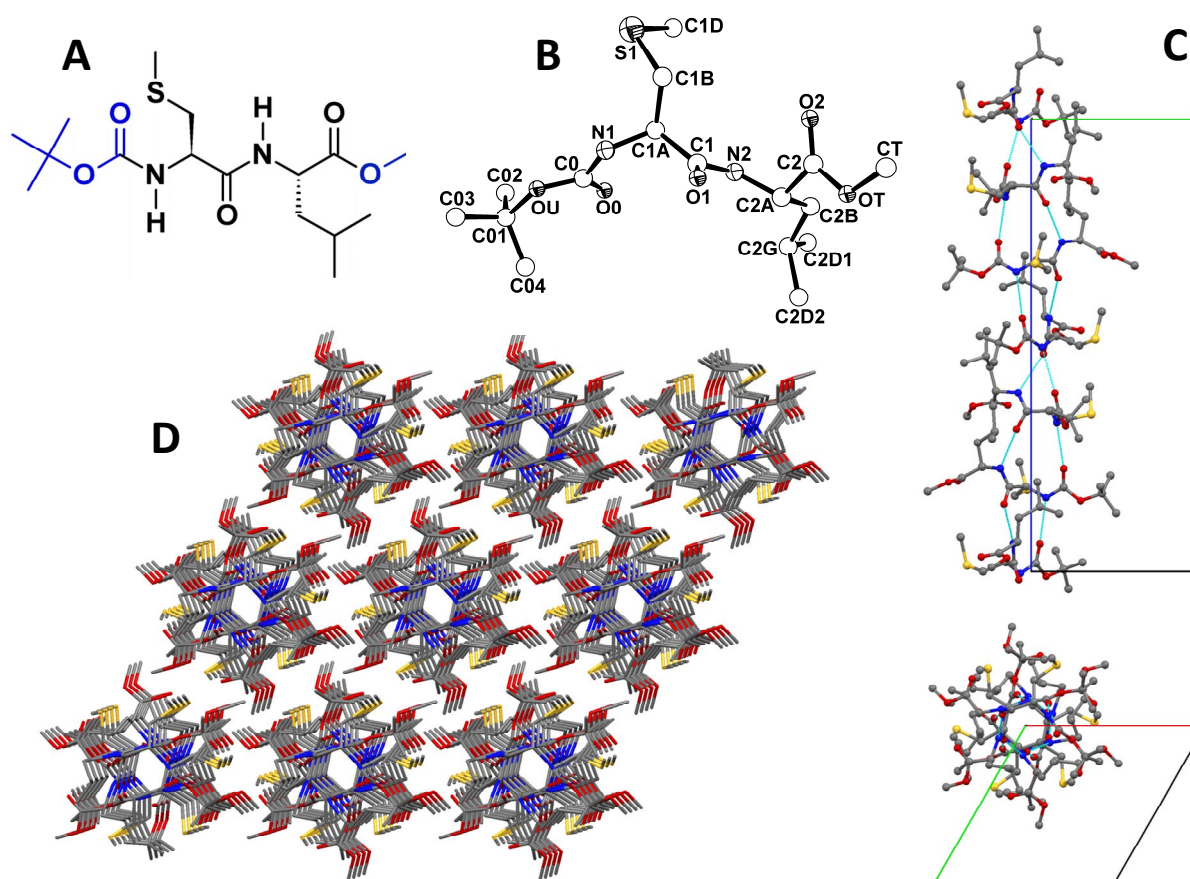


Fig. 1 (A) Chemical formula of dipeptide **1**. (B) X-Ray diffraction structure of **1** with atom numbering. (C) Packing mode of **1** in the crystal. Intermolecular H-bonding generates helical rows of molecules (see text for details). A single row is shown as viewed perpendicular (upper part) and parallel (lower part) to the sixfold screw axis. Intermolecular H-bonds are indicated by dashed lines. (D) Overall packing of **1** molecules as viewed nearly along the *c* axis. Carbon, grey; nitrogen, blue; oxygen, red; sulphur, yellow.

3.2 Self-assembly and gold nanoparticles inclusion

Dipeptide **1** is able to adopt a well-organized, micro-arrangement when allowed to self-assemble under appropriate conditions. Upon slow evaporation of concentrated solutions of **1** in either EtOAc (ethyl acetate), CH₃CN or acetone, long, aligned rods (up to 10 cm in length) are formed as shown in Figure 2A. Interestingly, such rods are characterized by an overall parallelepiped shape and present an empty inner cavity (Figure 2B).

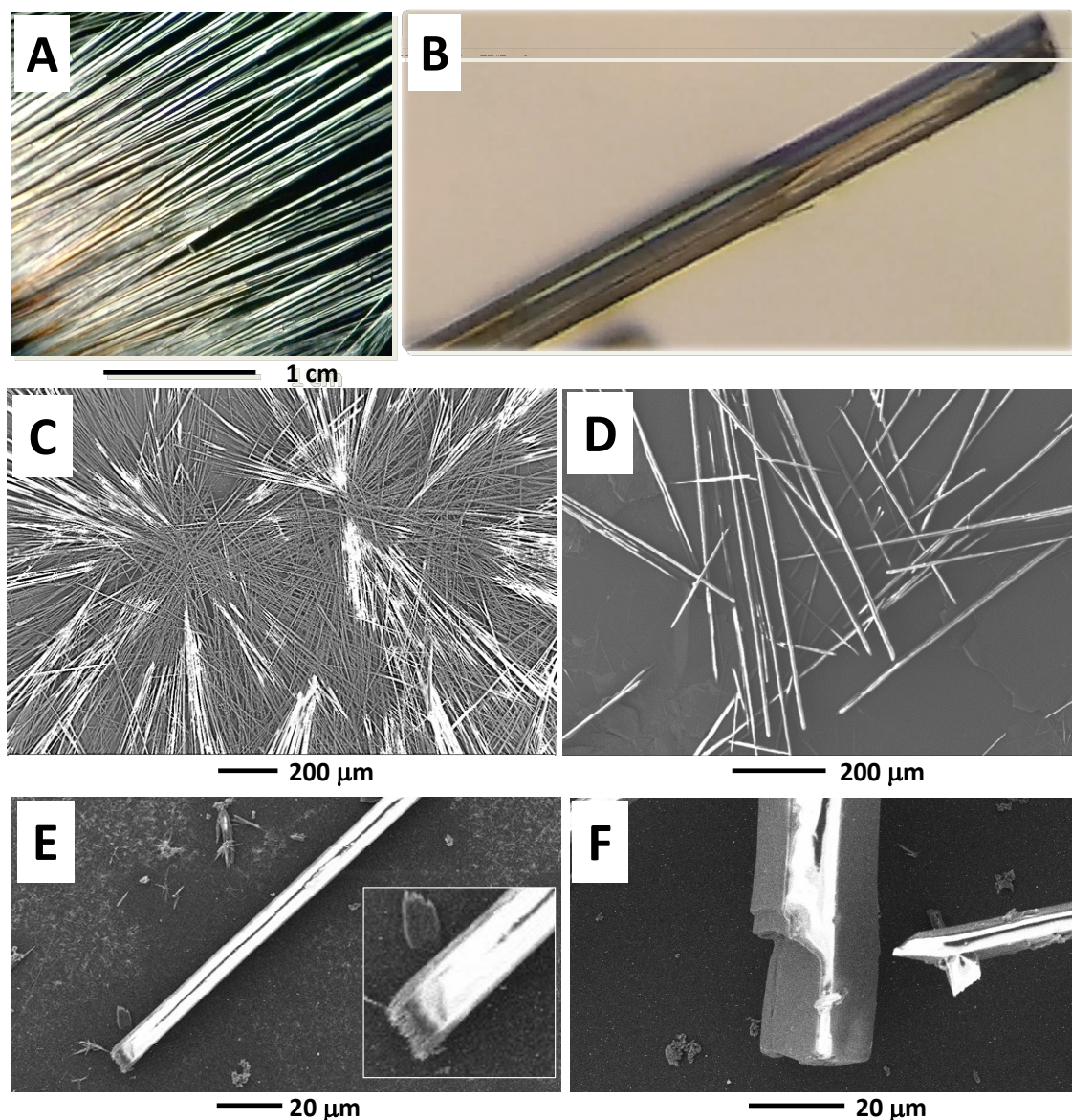


Fig. 2 (A) Camera picture of macroscopic rods from **1** obtained after evaporation from a concentrated solution in CH_3CN . (B) Camera picture showing details of a macroscopic rod obtained from a CH_3CN solution. (C) SEM image of micrometric rods from **1** obtained from a water/EtOAc interfacial crystallization. (D) SEM image of micrometric rods from **1** obtained from a water/MeOH solution. (E,F): SEM images showing details of the rods (obtained from a water/MeOH solution).

Smaller and packed rods of **1** (at the microscale level) were obtained by interfacial crystallization between water and EtOAc, as revealed by SEM images (Figure 2C). Moreover, by adding a diluted solution of **1** in MeOH to a large excess of water, formation of

micrometric, isolated rods was observed (Figure 2D). According to a SEM analysis (Figures 2E and 2F), even at this microscale level, the rods are characterized by an empty inner cavity while maintaining the overall parallelepiped shape found at the macroscale level.

Peptide **1** was further studied by circular dichroism (CD) in CH₃CN solution and as solid-state rods obtained after evaporation from the same solvent (Figures 3A and 3B). Notably, **1** shows a strong aggregation propensity in CH₃CN solution at concentrations above 1 mg/ml (Figure 3A). This conclusion is justified by the change of the Cotton effect near 195 nm from weakly positive at 0.3 mg/ml concentration to strongly negative at concentrations in the range 2.0 – 10 mg/ml, accompanied by a marked increase in ellipticity of the positive Cotton effect at about 218 nm. The CD spectra of the most concentrated solutions nicely resemble the spectrum obtained in the solid state (Figure 3B), *i.e.* that of the rod structure, although the latter would be entirely red-shifted, albeit slightly.

The powder X-ray diffraction (PXRD) technique was exploited in order to check whether formation of rods characterized by an empty cavity at the macro- and microscale level (prepared from CH₃CN and MeOH/water, respectively) could be ascribed to a supramolecular organization different from that determined at the single crystal level. The PXRD patterns of the rods prepared by the two methods (CH₃CN and MeOH/water) are identical to each other all over the 2θ range investigated, and virtually overlapping to the simulated pattern of the single crystal X-ray diffraction sample (Figure 3C). In addition, the values of the unit cell parameters extracted from the two experimental PXRD patterns are in excellent agreement with those of the single crystal (Table 1). These results clearly indicate that, although different preparation methods lead to different morphologies, the 3D-supramolecular organization adopted by **1** in the crystal state is shared by the micro- and macro-hollow rods. Similar conclusions were extracted from a Raman study (Figure 3D). Indeed, the rods obtained from the EtOAc/water and CH₃CN preparation methods exhibit identical Raman signatures.

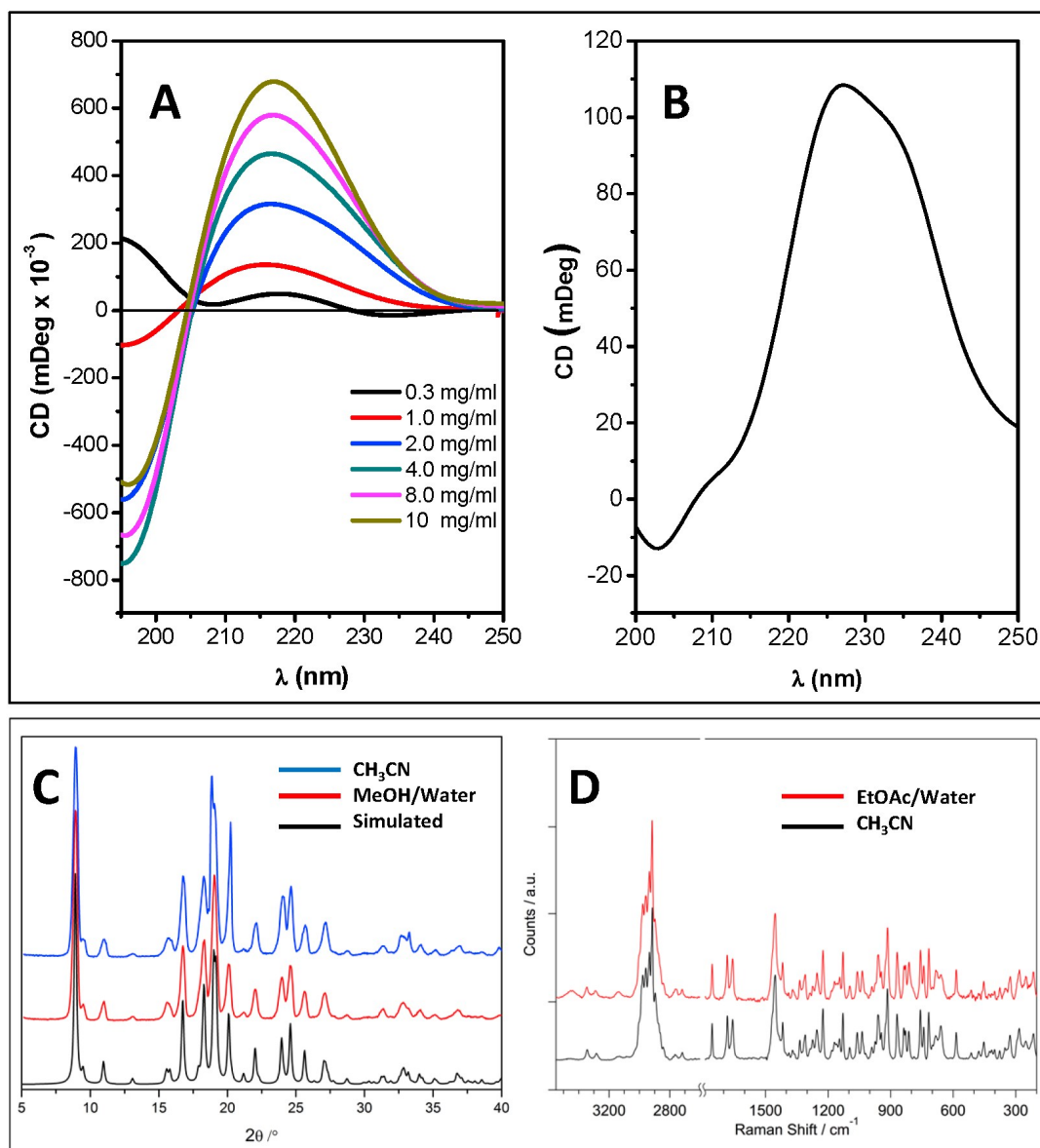


Fig. 3 (A) CD spectra of **1** at different concentrations in CH_3CN solution. (B) Solid-state CD spectra of rods obtained from CH_3CN . (C) Comparison of simulated PXRD measurements (from single-crystal X-ray diffraction) with experimental results on rods obtained from the CH_3CN and MeOH/water preparation methods. (D) Comparison of Raman spectra of the rods obtained from the EtOAc/water and CH_3CN preparation methods.

Table 1. Unit cell parameters of the single crystal structure of **1** and those extracted from powder pattern indexing of rods obtained from different preparation methods.

	a (Å)	b (Å)	c (Å)	α	β	γ	volume (Å ³)
Single crystal	11.4458(2)	11.4458(2)	27.7551(5)	90	90	120	3148.95(10)
MeOH/water	11.468(4)	11.468(4)	27.810(16)	90	90	120	3167(2)
CH ₃ CN	11.426(4)	11.426(4)	27.847(28)	90	90	120	3148(3)

To gain in-depth information on the nature of the rod architectures, we investigated the mother liquor remained after the MeOH/water preparation method. The transmission electron microscopy (TEM) analysis of this mixture carried out on stained (uranyl acetate) samples showed the presence of nano- and micrometric rods (Figure 4A).

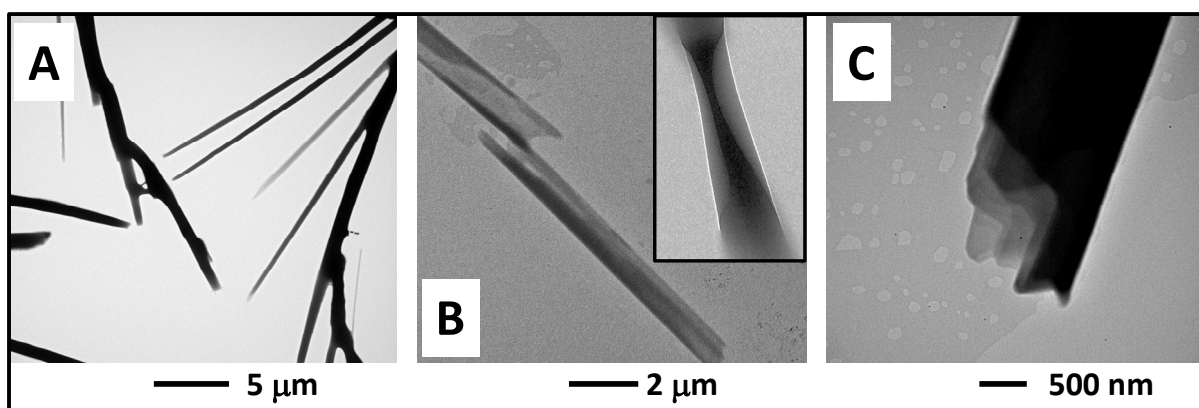


Fig. 4 (A) Stained TEM image after filtration of the macroscopic rods from a MeOH/water solution of **1**. (B) Stained TEM image showing details of the self-assembled rods. (C) Stained TEM image showing details of the multiwall nature of a nanoscopic rod.

A more detailed investigation of these samples revealed two interesting features. First, we observed the presence of “incompletely folded” rods, which confirmed the tubular nature of such type of architecture (Figure 4B). Secondly (Figure 4C), we noticed a multilayer structure of the external part of the rod. In a few cases, our TEM analysis of the same, but non-stained, sample (Figure 5A) revealed the typical structure of a multiwall nanotube characterized by two parallel, dark lines, associated to a higher material density, occurring at the boundaries of the rods. Interestingly, these images are similar to those that can be obtained from the TEM analysis performed on MWCNTs samples.³² To prove the existence of such a type of hollow

superstructure, we made use of citrate-passivated (water soluble) gold nanoparticles (10-nm diameter)³³ which were added to the MeOH/water solution. After the self-assembly process, the results of TEM analysis (non-stained samples, Figure 5B), energy-dispersive X-ray spectroscopy (EDX) (Figure 5C), and optical microscopy (polarized light, Figures 5D and 5E) clearly showed that the gold nanoparticles are incorporated into the rod structures.

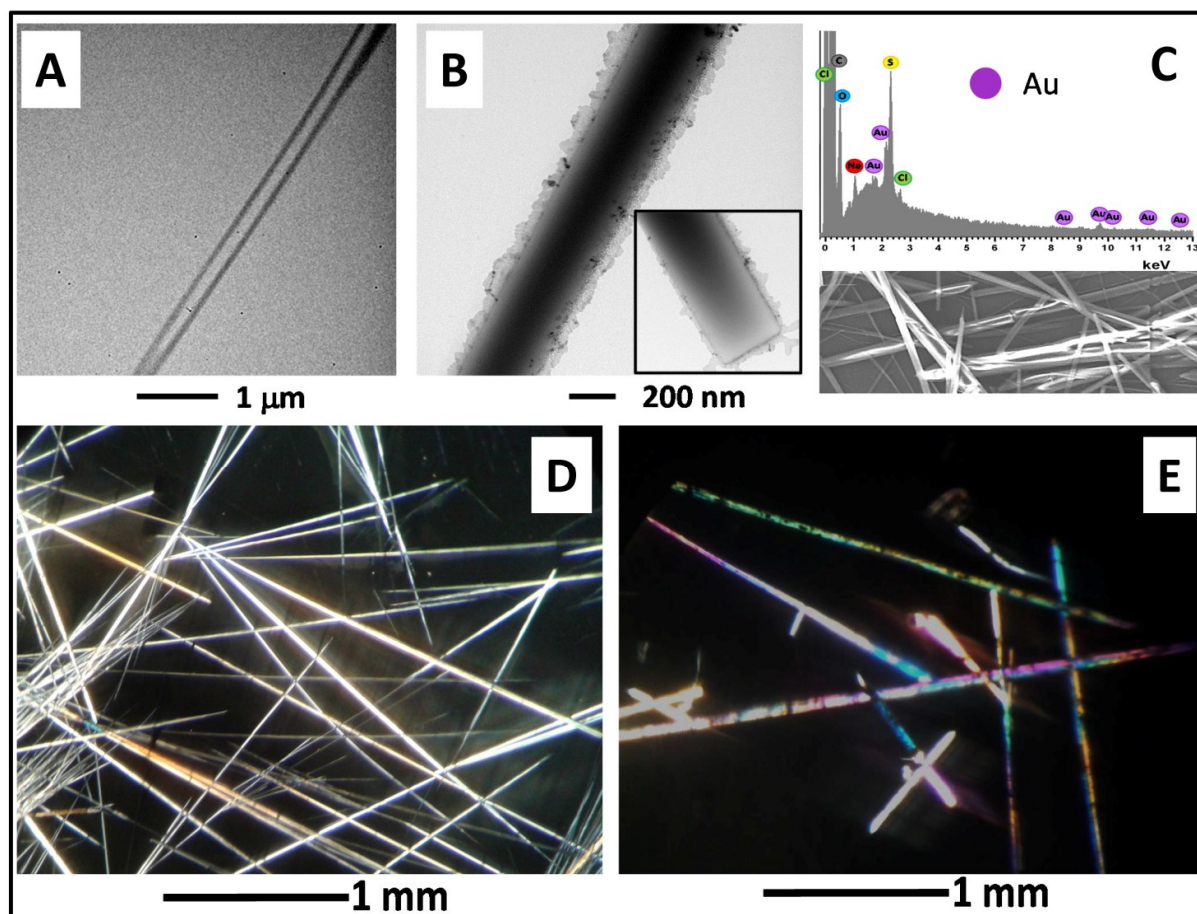


Fig. 5 (A) Non-stained TEM image of a nanorod of **1**. (B) Non-stained TEM image showing the encapsulation of water-soluble gold nanoparticles into a rod. (C) SEM image and EDX pattern of the **1**-nanotube / gold nanoparticles hybrid rods. (D) Optical microscopy image of **1**-rods prepared from MeOH/water under polarized light. (E) Optical microscopy image of co-assembled **1**-rods/gold nanoparticles under polarized light.

Interestingly, we found that **1** is able to interact with citrate-passivated gold nanoparticles, probably via its thioether sulfur atom, resulting in self-aggregation of the nanoparticles. This hypothesis is supported by comparison of the TEM images (Figure 6A and 6B) and the UV-

vis absorption spectra (Figure 6C) of the citrate-passivated gold nanoparticles and the **1**-passivated gold nanoparticles. The strong aggregation occurring for **1**-passivated gold nanoparticles results in a remarkable red-shift of its plasmonic band as compared with that of the citrate-passivated gold nanoparticles. Moreover, the CD spectra of the **1**-passivated gold nanoparticles (Figure 6D) showed a chiral signature in correspondence to the plasmonic region (400-600 nm), that may arise from the interactions of **1** (which is a chiral molecule) with the gold core. A similar chiral signature of the plasmonic band was previously reported for a 10-nm gold nanoparticle-peptide conjugate.³⁴

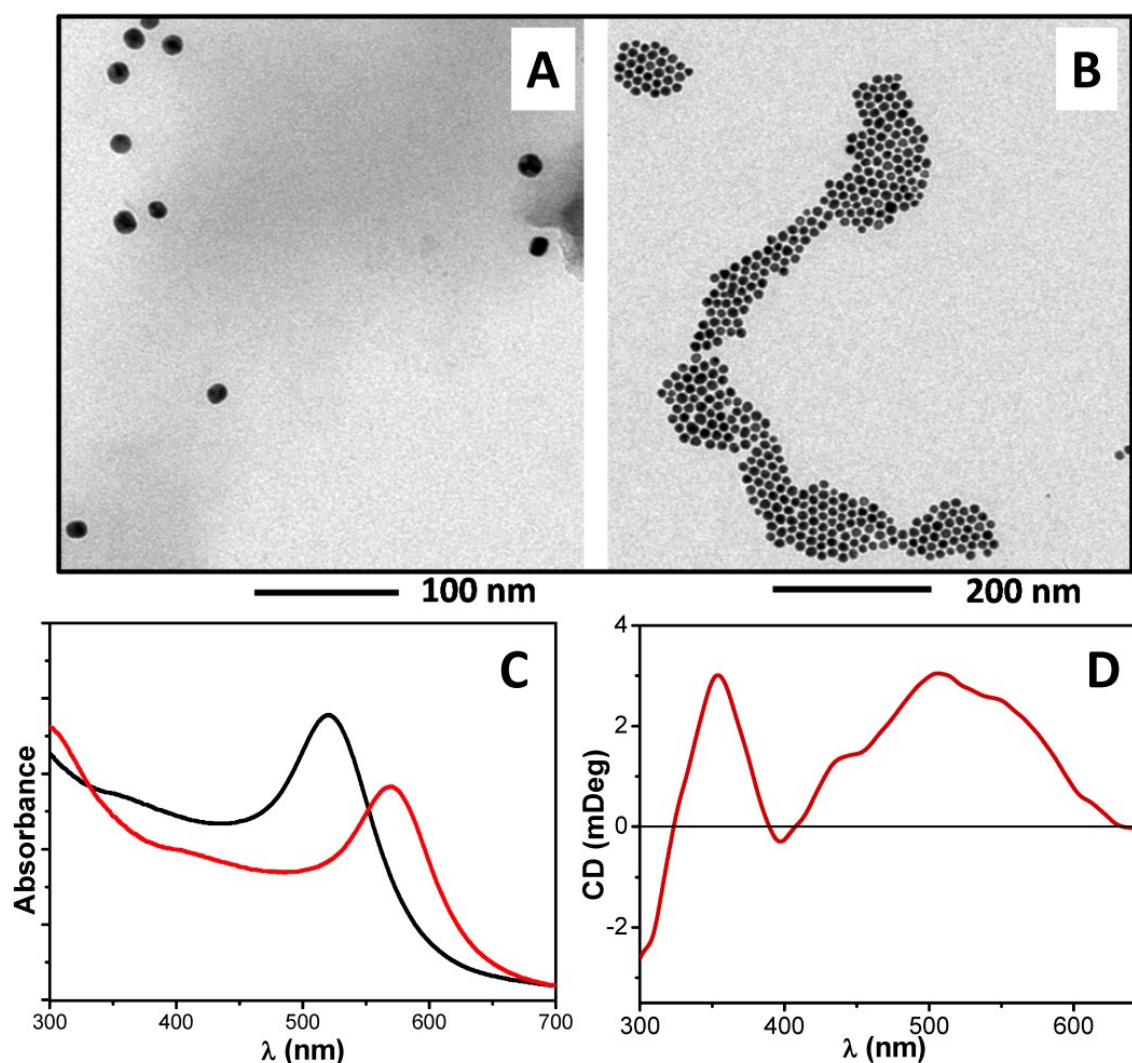


Fig. 6 (A) TEM image of citrate-passivated gold nanoparticles. (B) TEM image of **1**-passivated gold nanoparticles. (C) UV-vis absorption spectra of citrate-passivated gold

nanoparticles (black line) and **1**-passivated gold nanoparticles (red line). (D) CD spectra of **1**-passivated gold nanoparticles.

In addition, treatment at 400 °C in oxygen atmosphere of the co-assembled **1**-rods/gold nanoparticles described above led to the formation of gold nanorods (about 100-200 nm in length) as detected by TEM (Figures 7A and 7B). The UV-vis absorption spectrum of this material (Figure 6C) is characterized by a relatively sharp band at about 525 nm, accompanied by a much broader absorption centered near 720 nm, features typical of gold nanorods.³⁵

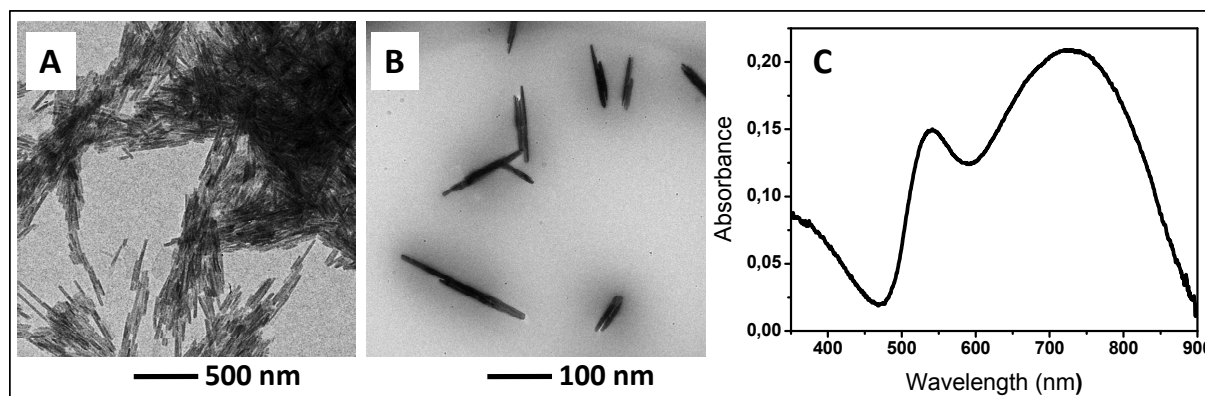


Fig. 7 (A) and (B) TEM images of gold nanorods, obtained by treatment at 400 °C in oxygen atmosphere of the the co-assembled **1**-rods/gold nanoparticles, recorded prior and after a sonication process, respectively. (C) UV-vis absorption spectra of gold nanorods in aqueous suspension.

3.3 Organogel formation

To further expand our study of the self-assembly propensity of **1** in organic solvents, we prepared a set of concentrated solutions of **1** in toluene. We observed formation of organogel (after a gentle heating followed by a cooling process) when solutions of **1** reach the concentration of 85 mg/ml. According to a TEM analysis, the organogel is characterized by a dense network composed by long (up to 10 μm) and twisted fibers (Figures 8A and 8B).

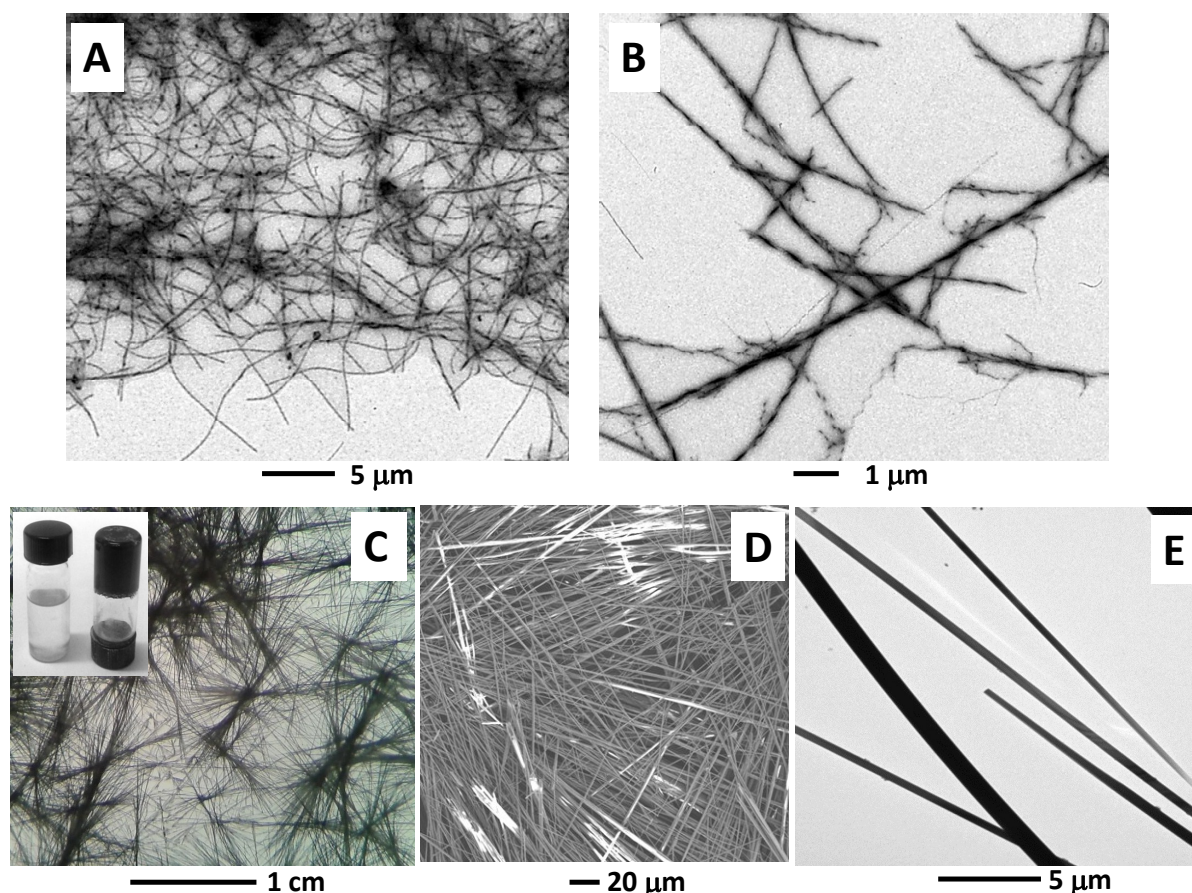


Fig. 8 (A and B) Stained TEM images showing the organogel microstructure (fibers) of **1** and details of the twisted nature of the fibers. (C) Optical microscopy image of the **1**/MWCNTs organogel obtained after evaporation of toluene. Inset: Vials showing a 85 mg/ml solution of **1** in toluene at 70 °C (left) and the corresponding organogel formed after sonication in the presence of MWCNTs and cooling to room temperature (right; the vial is upside down). (D) and (E): SEM and non-stained TEM images, respectively, of the **1**/MWCNTs composite obtained after evaporation of toluene.

3.4 Multicomponent organogels

Addition of MWCNTs to a solution of **1** (85 mg/ml) in toluene, followed by sonication, allowed us to obtain **1**/MWCNTs organogel systems (Figure 8C, inset). Once deposited on a glass surface, this organogel rapidly crystallized in microscopic black needles, as detected by optical microscopy and SEM (Figures 8C and 8D, respectively). Moreover, small and large nanostructures were unraveled also by TEM (Figure 8E). A comparison of the TEM analyses of the organogel formed by **1** alone (stained sample, Figures 8A and 8B) and of the

1/MWCNTs organogel (non-stained sample, Figure 8E), indicates a much higher matter density for the latter. This finding suggests that in the **1**/MWCNTs organogel the MWCNTs might have been incorporated, and probably ordered, within the rods. We found that addition of a 15% v/v MeOH (a good solvent for **1**, but not for MWCNTs) was successful in disassembling the **1**/MWCNTs organogel system, resulting in a black MWCNTs precipitate and a colorless solution (the same effect was also observed after addition of ethanol, isopropanol, CH₃CN and N,N-dimethylformamide). Therefore, we decided to progressively disrupt the rods directly on the TEM-grid by adding increasing amounts of MeOH or CH₃CN to the **1**/MWCNTs organogel drop prior to TEM detection. The resulting TEM images are reported in Figure 9. In particular, by comparing the TEM images reported in Figure 8E (needles obtained by evaporation) and Figure 9A (needles after addition of 0.5% MeOH) it seems clear that addition of MeOH affects the overall morphology. Subsequent additions of larger amounts of MeOH resulted in the collapse of the needle morphology (Figures 9B and 9C). This finding was also observed upon addition of CH₃CN (Figures 9D and 9E). In particular, Figures 9A-9E show formation of packed (or single) strands (between a 30-100 nm width, and up to a 5- μ m length) that originate from the needle structures mentioned earlier. Our most relevant observation is that strands are detected on a non-stained sample, which suggests a high matter density occurring in these superstructures. We hypothesize that these strands are related to the **1**-MWCNTs co-assembled systems where the MWCNTs surfaces are covered by **1**.

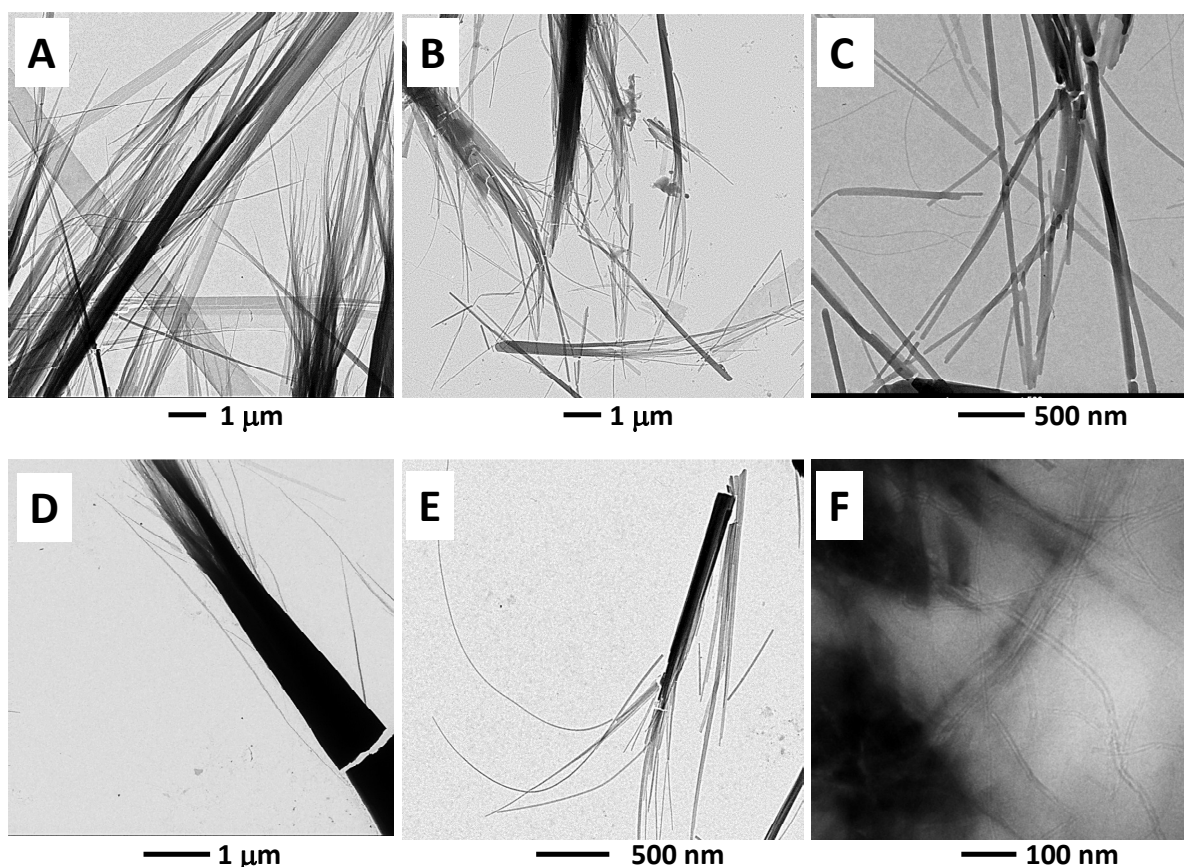


Fig. 9 Non-stained TEM images showing the effect of the addition of MeOH (A-C) or CH₃CN (D,E) to the 1/MWCNTs organogel microstructure on the TEM-grid. Specifically: additions of 0.5% (A), 2% (B) and 5% (C) MeOH (v/v); additions of 1% (D) and 3% (E) CH₃CN (v/v). (F) Non-stained TEM image after sonication of MWCNTs in a solution of 1 at 10 mg/ml in toluene.

As a control experiment, we prepared a solution of 1 at the concentration of 10 mg/ml in toluene and added MWCNTs. Under these conditions, after a sonication process, no microstructures were formed. However, it was possible to detect (by TEM) partially unbundled MWCNTs (Figure 9F). The latter observation is an important evidence for the co-assembly propensity of 1 with MWCNTs. Thus, 1 seems to be able to partially disperse MWCNTs in toluene solution. Overall, we can likely assume that formation of 1/MWCNTs co-assembled needles goes through a series of steps. Specifically, MWCNTs are first covered by 1, then MWCNTs become disperse in the solution media, and eventually the covered 1-

MWCNTs complexes align (with the support of the large excess of **1**) giving rise to the supramolecular hybrid architectures.

Moreover, addition of C_{60} to a solution of **1** (85 mg/ml) in toluene, followed by sonication, allowed us to obtain $1/C_{60}$ organogel systems (Figure 10A, and inset). Inspection of a diluted $1/C_{60}$ organogel sample deposited on the TEM grid revealed the presence of small particles (from 5- to 15-nm in diameter) spread all over the organogel network (Figure 10B). These particles are possibly due to formation of C_{60} aggregates. The $1/C_{60}$ organogel, once deposited on a glass surface, rapidly crystallized in microscopic red/orange needles (Figure 10C inset) that were characterized by SEM (Figure 10C).

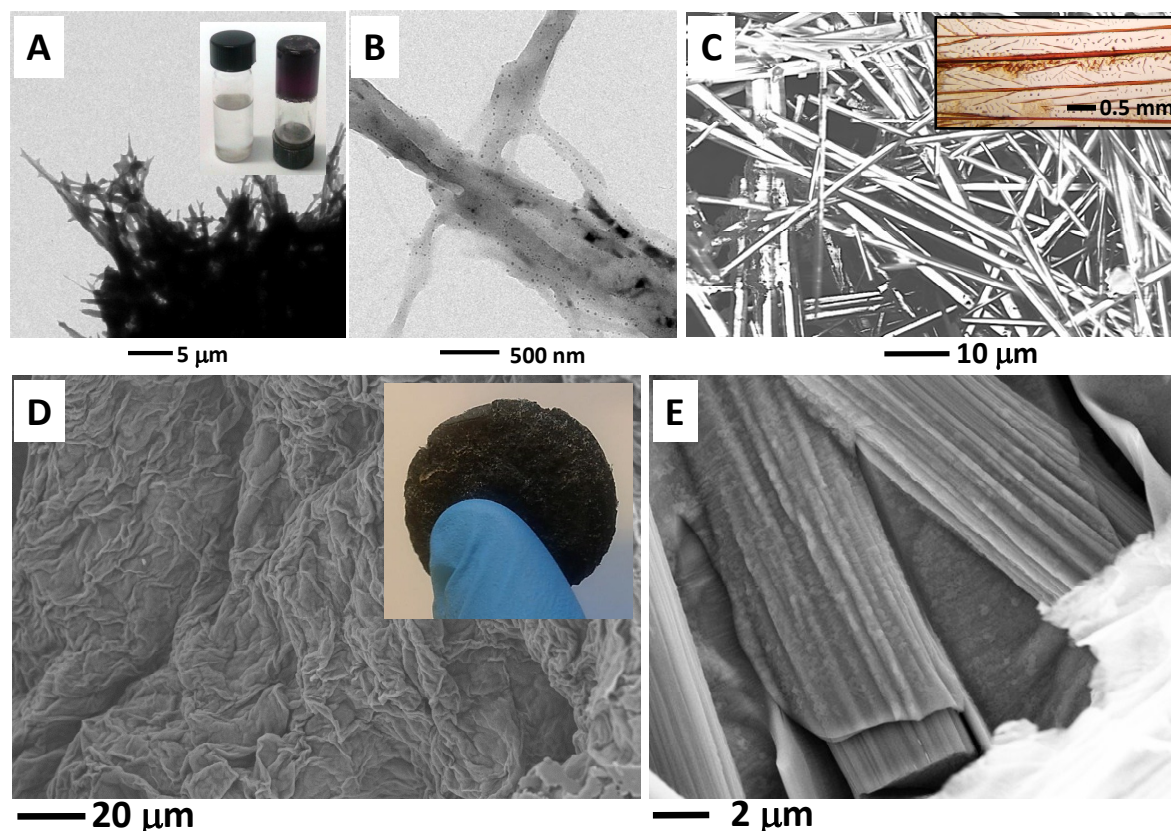


Fig. 10 (A) Non-stained TEM images showing the $1/C_{60}$ organogel microstructure (formed in toluene). Inset: Vials showing a 85 mg/ml solution of **1** in toluene at 70 °C (left) and the corresponding organogel formed after sonication in the presence of C_{60} and cooling to room temperature (right; the vial is upside down).. (B) TEM details showing the presence of small particles (in a diluted sample) incorporated into the microstructure network. (C) SEM image of the $1/C_{60}$ organogel microscopic needles obtained after rapid crystallization. Inset: camera

picture of microscopic red/orange needles. (D) SEM image of the 1/C₆₀/MWCNTs composite obtained from the corresponding organogel in toluene after the high vacuum-drying process. Inset: camera picture of the 1/C₆₀/MWCNTs composite. (E) SEM details of the 1/C₆₀/MWCNTs composite showing the presence of ordered co-assembled rods.

The organogels formed by **1** alone, 1/C₆₀, and 1/MWCNTs are characterized by a transition temperature for the sol-gel process ($T_{\text{sol-gel}}$) of 55, 47, and 85 °C, respectively. These data indicate that, in comparison to **1**, the gel stability is only marginally affected by the presence of fullerene, but it is strongly increased by MWCNTs.

3.5 Three-component catalyst

With the aim at preparing a robust material with catalytic properties, we decided to combine the 1/C₆₀ and 1/MWCNTs carbon-based organogels. In particular, the two gels were melted in their sol (liquid) forms and combined together. After a sonication process followed by standing at room temperature, a novel 1/C₆₀/MWCNTs organogel was obtained, which displayed a $T_{\text{sol-gel}}$ of 79 °C. Removal of the solvent by a high vacuum-drying process at room temperature afforded a mechanically robust self-assembled solid material, characterized by a high porosity (300 mg of the material prepared by this process occupy as many as 6 cm³) and insoluble in water (Figure 10D, and inset). The vacuum-drying process itself helps keeping the gel size, because the fast evaporation procedure used generates a low temperature. The consequent gel hardening at low temperature is beneficial to retain the size. Furthermore, the fast drying process shortens the time allowed to capillary forces to act on the gel, thus moderating the structure collapse caused by strain accumulation.³⁶ The SEM details reported in Figure 10E showed the presence of co-assembled rods which exhibit ordered and aligned domains on their surfaces. Remarkably, the same processes performed on the **1** or 1/C₆₀ organogels did not provide any organized material. The interest for nanocarbon materials as catalysts is rapidly growing, as highlighted by recent review articles.^{37,38} In this connection,

Khashab and coworkers³⁹ reported the successful reduction of a set of azo compounds to the corresponding aromatic amines by NaBH₄ under UV irradiation in basic water using C₆₀ as the catalyst. It is known that NaBH₄ is unable to reduce the azo group without the assistance of a metal catalyst, such as Pd or Ag.^{40,41} The catalytic effect of C₆₀ was ascribed to the electron acceptor properties of its UV-promoted triplet state, which lead to activation of the N=N bond. The limitations of such a system are related to the insolubility of C₆₀ in water, which results in its poor dispersion and formation of large aggregates. Indeed, 10 mg of C₆₀ were required in order to catalyze the reduction of 10 mg of methyl orange after 5 hours under illumination in the presence of a large excess of NaBH₄.³⁹ We envisioned that our 1/C₆₀/MWCNTs hybrid material could be a more efficient catalyst than C₆₀ alone in the reduction of azo compounds. Actually, by using 100 mg of the 1/C₆₀/MWCNTs self-assembled solid material (which contains approximately 2.5 % w/w of C₆₀) and 100 mg of NaBH₄, quantitative conversion of 200 mg of either methyl orange, methyl red, or 4-aminoazobenzene to the corresponding amines was achieved within 45 minutes under UV irradiation at 365 nm in water. The water-insoluble catalyst was easily recovered by filtration. Chemical selectivity was observed as indicated in Figure 11, which was identical to that reported in the previous study.³⁹ A comparison of our results with those reported for the same reaction by Khashab and coworker³⁹ strongly supports the view that in our catalyst C₆₀ is molecularly well dispersed on a large porous surface, thus allowing a more effective interaction with the azo compounds. These findings prompted us to explore additional potential applications for our 1/C₆₀/MWCNTs co-assembled solid material as a catalyst in NaBH₄-mediated reduction reactions. NaBH₄ is commonly used to reduce aldehydes and ketones to give the related alcohols, but is not reactive enough to reduce carboxylic acids or esters. We found that, under experimental conditions closely related to those exploited for the reduction of azo compounds, our catalyst is able to promote the reduction of benzoic acid to benzyl alcohol (4 hours, 96% conversion, see *Supporting Information*).

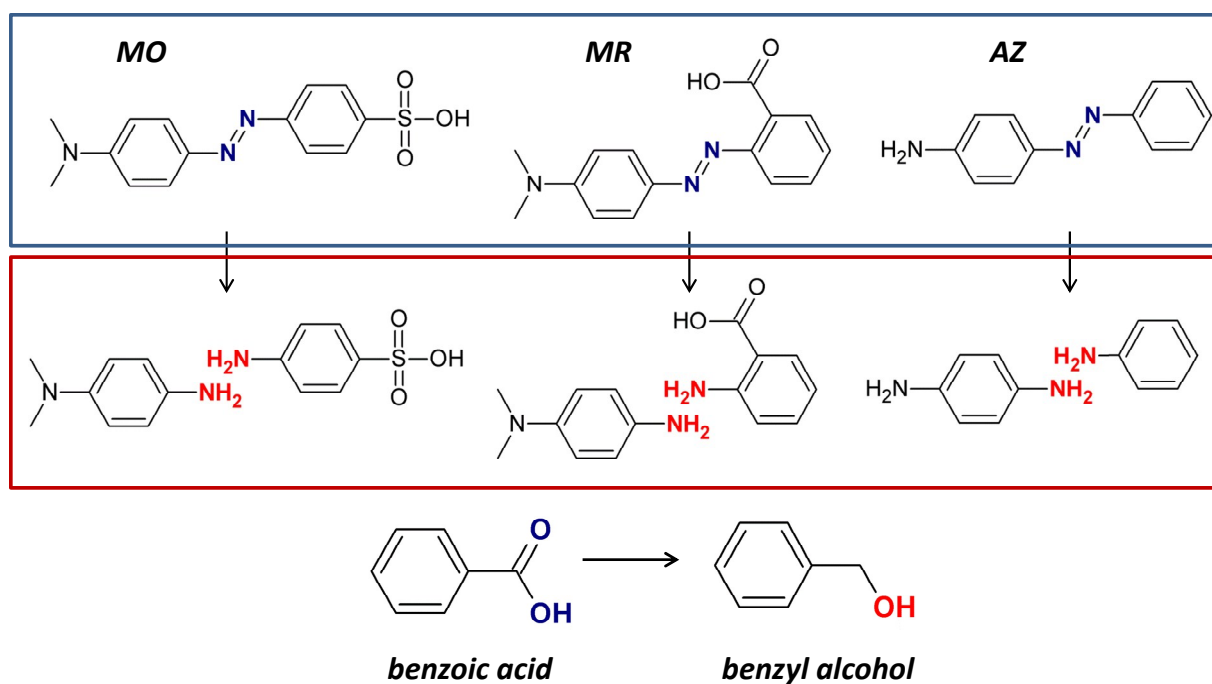


Fig. 11 Chemical structures of methyl orange (MO), methyl red (MR), 4-amino-azobenzene (AZ), and benzoic acid, and the corresponding products of reduction reactions.

It has to be noted that although methyl red carries a carboxylic group, its NaBH_4 -mediated reduction reaction catalyzed by our $1/\text{C}_{60}/\text{MWCNTs}$ co-assembled solid material did not lead to any detectable formation of *ortho*-aminobenzyl alcohol. In this case the effects of the amino substituent at the *ortho* position prevent the reduction of the carboxylic function under our experimental conditions.

4. Conclusion

To summarize, we have shown that a *terminally protected*, hydrophobic dipeptide, Boc-L-Cys(Me)-L-Leu-OMe (**1**), is able to hierarchically self-assemble in well-defined structures. In particular, evaporation from organic solvents (*e.g.*, EtOAc, CH_3CN , acetone) or interfacial (EtOAc/water and MeOH/water) crystallizations led to the formation of hollow rods ranging from the nano- to the macroscale. In addition, an organogel could be obtained using toluene, the microstructure of which is characterized by twisted fibers. The organogel of **1** formed in

the presence of C₆₀ or MWCNTs shows a different morphology (needles). Evidence is provided in support of the view that **1**, besides helping in dispersing the otherwise insoluble MWCNTs, is able to co-assemble with them. We succeeded in obtaining a novel ternary, co-assembled, carbon-based material by taking advantage of the self-assembly tendency of **1**. Specifically, by using a high vacuum-drying process, the **1**/C₆₀/MWCNTs organogel was converted into a robust, high-volume, water insoluble, solid material where C₆₀ is well dispersed over the entire superstructure. We exploited this new material as a catalyst in the reduction reaction of azo compounds (mediated by NaBH₄ and UV-light). Our material proved to perform remarkably better than C₆₀ alone in this reaction. Moreover, we extended its usefulness to a novel application, namely the reduction of benzoic acid to benzyl alcohol. Finally, it is worth recalling that most of the linear peptides reported to form nanotubes are characterized by the occurrence of a sixfold screw axis as a symmetry element in their crystal structures.^[18,19,23-26] This property is also shared by our *terminally protected* dipeptide Boc-L-Cys(Me)-L-Leu-OMe (**1**) that crystallizes in the hexagonal space group P6₅. However, at variance with **1**, its positional isomer Boc-L-Leu-L-Cys(Me)-OMe (**2**, see *Supporting Information*), that crystallizes in the orthorhombic space group P2₁2₁2₁, in our hands was unable to generate any superstructure, thus suggesting a strong connection between packing mode and self-assembly behavior. Interestingly, quite recently a strictly related observation was published, namely that sequence exchange in an *unprotected* dipeptide (Val-Ala vs. Ala-Val) strongly affects its molecular structure and the related self-assembly tendency.⁴²

Supplementary Information (ESI) available: Synthetic details, X-ray crystal structural analysis CCDC 1057628 (1) and 1057629 (2) and catalysis results.

Acknowledgements

The authors thank Dr. F. Bertasi for Raman spectra technical support. Financial support from the University of Padova (PRAT C91 J11003560001) is gratefully acknowledged.

References

- [1] J. M. Lehn, *Angew. Chem. Int. Ed.*, 1988, **27**, 89-112.
- [2] J. M. Lehn, *Angew. Chem. Int. Ed.*, 1990, **29**, 1304-1319.
- [3] J. M. Lehn, *Science*, 1993, **260**, 1762-1763.
- [4] J. M. Lehn, *Science*, 2002, **295**, 2400-2403.
- [5] J. M. Lehn, *Proc. Natl. Acad. Sci. USA*, 2002, **99**, 4763-4768.
- [6] G. M. Whitesides and B. Grzybowski, *Science*, **2002**, 295, 2418-2421.
- [7] E. Gazit, *Chem. Soc. Rev.*, 2007, **36**, 1263-1269.
- [8] A. Rui, A. Mendes and L. Gales, *J. Mater. Chem.*, 2012, **22**, 1709-1723.
- [9] R. Chapman, M. Danial, M. L. Koh, K. A. Jolliffe and S. Perrier, *Chem. Soc. Rev.*, 2012, **41**, 6023-6041.
- [10] T. D. Clark, L. K. Buehler and M. R. Ghadiri, *J. Am. Chem. Soc.*, 1998, **120**, 651-656.
- [11] X. Y. Gao and H. Matsui, *Adv. Mater.*, 2005, **17**, 2037-2050.
- [12] Z. Luo and S. Zhang, *Chem. Soc. Rev.*, 2012, **41**, 4736-4754.
- [13] C. Valéry, F. Artzner and M. Paternostre, *Soft Matter*, 2011, **7**, 9583-9594.
- [14] X. Yan, P. Zhu, J. Li, *Chem. Soc. Rev.*, 2010, **39**, 1877-1890.
- [15] I. W. Hamley, *Angew. Chem. Int. Ed.*, 2007, **46**, 8128-8147.
- [16] M. Mba, A. Moretto, L. Armelao, M. Crisma, C. Toniolo and M. Maggini, *Chem. Eur. J.*, 2011, **17**, 2044-2047.
- [17] M. Mba, A. I. Jiménez and A. Moretto, *Chem. Eur. J.*, 2014, **20**, 3888-3893.
- [18] C. H. Görbitz, *Chem. Commun.*, 2006, 2332-2334.
- [19] C. H. Görbitz, *Chem. Eur. J.*, 2007, **13**, 1022-1031.
- [20] A. K. Das, D. Haldar, R. P. Hedge, N. Shamala and A. Banerjee, *Chem. Commun.*, 2005, 1836-1838.
- [21] P. P. Bose, A. K. Das, R. P. Hedge, N. Shamala and A. Banerjee, *Chem. Mater.*, 2007, **19**, 6150-6157.
- [22] M. Reches and E. Gazit, *Science*, 2003, **300**, 625-627.

- [23] S. Ray, D. Haldar, M. G. B. Drew and A. Banerjee, *Org. Lett.*, 2004, **6**, 4463-4465.
- [24] M. Crisma, C. Toniolo, S. Royo, A.I. Jiménez and C. Cativiela, *Org. Lett.*, 2006, **8**, 6091-6094.
- [25] U. S. Raghavender, Kantharaju, S. Aravinda, N. Shamala and P. Balaram, *J. Am. Chem. Soc.*, 2010, **132**, 1075-1086.
- [26] U. S. Raghavender, B. Chatterjee, I. Saha, A. Rajagopal, N. Shamala and P. Balaram, *J. Phys. Chem. B*, 2011, **115**, 9236-9243.
- [27] M. C. Burla, M. Camalli, B. Carrozzini, G. L. Cascarano, C. Giacovazzo, G. Polidori and R. Spagna, *J. Appl. Crystallogr.*, 2003, **36**, 1103.
- [28] G. M. Sheldrick, *Acta Crystallogr.*, 2008, **A64**, 112-122.
- [29] A. Altomare, G. Campi, C. Cuocci, L. Eriksson, C. Giacovazzo, A. Moliterni, R. Rizzi and P.-E. Werner, *J. Appl. Crystallogr.*, 2009, **42**, 768-775.
- [30] A. Altomare, C. Cuocci, C. Giacovazzo, A. Moliterni, R. Rizzi, N. Corriero and A. Falcicchio, *J. Appl. Crystallogr.*, 2013, **46**, 1231-1235.
- [31] Crystal data for Boc-L-Cys(Me)-L-Leu-OMe: $C_{16}H_{30}N_2O_5S$; $M = 362.48$, hexagonal, $a = b = 11.4458(2)$, $c = 27.7551(5)$ Å, $V = 3148.95(10)$ Å³, $T = 293(2)$ K, space group $P6_5$, $Z = 6$, 18290 reflections measured, 2281 independent reflections ($R_{int} = 0.044$), $R_1 = 0.0403$ [$F \geq 4\sigma(F)$], $wR_2 = 0.1083$ (F^2 all data), goodness-of-fit on $F^2 = 1.042$. Flack parameter -0.01(3). CCDC 1057628.
- [32] A. Bianco, K. Kostarelos, C. D. Partidos and M. Prato, *Chem. Commun.*, 2005, 571-577.
- [33] G. Frens, *Nature Phys. Sci.*, 1973, **241**, 20-22.
- [34] J. M. Slocik, A. O. Govorov and R. R. Naik, *Nano Lett.*, 2011, **11**, 701-705.
- [35] Y. Ying, S. S. Chang, C.L. Lee and C. R. C. Wang, *J. Phys. Chem. B*, 1997, **101**, 6661-6664.
- [36] Z. Wang, Z. Dai, J. Wu, N. Zhao and J. Xu, *Adv. Mater.*, 2013, **25**, 4494-4497.
- [37] D. R. Dreyer and C. W. Bielawski, *Chem. Sci.*, 2011, **2**, 1233-1240.
- [38] D. S. Su, S. Perathoner and G. Centi, *Chem. Rev.*, 2013, **113**, 5782-5816.
- [39] Y. Guo, W. Li, J. Yan, B. Moosa, M. Amad, C. J. Werth and N. M. Khashab, *Chem. Asian J.*, 2012, **7**, 2842-2847.
- [40] L. Kong, X. Lu, X. Bian, W. Zhang and C. Wang, *ACS Appl. Mater. Interfaces*, 2011, **3**, 35-42.

- [41] N. Gupta, H. P. Singh and R. K. Sharma, *J. Mol. Catal. A, Chem.*, 2011, **335**, 248-252.
- [42] H. Erdogan, E. Babur, M. Yilmaz, E. Candas, M. Gordesel, Y. Dede, E. E. Oren G. B. Demirel, M. K. Ozturk, M. S. Yavuz and G. Demirel, *Langmuir*, 2015, **31**, 7337-7345.

An efficient catalyst for reduction chemistry in water was prepared by co-assembly of hydrophobic dipeptide, multiwall carbon nanotubes, and C₆₀.

